# Optical properties of Finnish lakes estimated with simple bio-optical models and water quality monitoring data

**Kari Kallio**

Finnish Environment Institute, PO Box 140, 00251 Helsinki, Finland. E-mail: *kari.y.kallio@ymparisto.fi*

Received 7 January 2005; accepted in revised form 15 November 2005

**Abstract** The aim of this study was to estimate the distributions of spectral diffuse attenuation coefficient, attenuation depth and subsurface reflectance of Finnish lakes. In addition, the optimum empirical water quality interpretation algorithms employing reflectance ratios were investigated for the needs of remote sensing. Estimations of the optical properties were based on simple optical models and measured concentrations of optically active substances (the sum of chlorophyll *a* and phaeophytin *a*, total suspended solids and coloured dissolved organic matter (CDOM)) at 1670 monitoring stations representing 1113 lakes. The models were parameterized using optical data from 10 lakes. The mean diffuse attenuation coefficient in PAR was 3.5 $m^{-1}$ and the location of the maximum attenuation depth was in the range 564–714 nm. The simulated reflectance spectra showed a shift of the maximum value to longer wavelengths as trophic status changed from oligotrophic to hyper-eutrophic. High CDOM concentrations decrease the estimation accuracy of chlorophyll *a* from reflectance spectra using empirical algorithms, particularly in oligotrophic lakes. The models described can be used in studying light availability for photosynthesis at different depths, in the simulation of water temperatures, in estimating how different management alternatives affect light attenuation and Secchi depth, and in various remote sensing applications.

**Keywords** Attenuation; lakes; optical models; reflectance; Secchi depth; water quality

Nordic Hydrology **Vol 37 No 2 pp 183–204** © IWA Publishing 2006

## Nomenclature

| | |
|---|---|
| $a_{cdom}(\lambda)$ | absorption coefficient of CDOM ($m^{-1}$) |
| $a_{cdom}(400)$ | absorption coefficient of CDOM at 400 nm ($m^{-1}$) |
| AOP | apparent optical property |
| $a_{ph}(\lambda)$ | absorption coefficient of phytoplankton ($m^{-1}$) |
| $a^*_{ph}(\lambda)$ | Chlorophyll *a* specific absorption coefficient of phytoplankton ($m^{-1}$) |
| $a_{Tot}(\lambda)$ | total absorption coefficient ($m^{-1}$) |
| $a_{Tri}(\lambda)$ | absorption coefficient of tripton ($m^{-1}$) |
| $a^*_{\underline{TSS}}$ | specific absorption coefficient of bleached total suspended solids ($l\,m^{-1}\,mg^{-1}$) |
| $a^*_{\underline{TSS}}(400)$ | specific absorption coefficient of bleached total suspended solids at 400 nm ($l\,m^{-1}\,mg^{-1}$) |
| $a_w(\lambda)$ | absorption coefficient of pure water ($m^{-1}$) |
| $b_{b,Tot}(\lambda)$ | total backscattering coefficient ($m^{-1}$) |
| $bp_w$ | backscattering probability of pure water |
| $bp_{TSS}$ | backscattering probability of TSS |
| $b_{Tot}(\lambda)$ | total scattering coefficient ($m^{-1}$) |
| $b^*_{TSS}(\lambda)$ | specific scattering coefficient of TSS ($l\,m^{-1}mg^{-1}$) |
| $b^*_{TSS}(555)$ | specific scattering coefficient of TSS at 555 nm ($l\,m^{-1}\,mg^{-1}$) |
| $b_w(\lambda)$ | scattering coefficient of pure water ($m^{-1}$) |
| $c_{Tot}(\lambda)$ | total beam attenuation coefficient ($m^{-1}$) |

doi: 10.2166/nh.2006.007

| | |
|---|---|
| CDOM | coloured dissolved organic matter |
| $C_{\text{Chl-a}}$ | concentration of the sum of chlorophyll *a* and phaeophytin *a* ($\mu g\,l^{-1}$) |
| $C_{\text{TSS}}$ | concentration of total suspended solids ($mg\,l^{-1}$) |
| $E_d(\lambda)$ | downwelling irradiance |
| $K_d(\lambda)$ | diffuse attenuation coefficient ($m^{-1}$) |
| $\mu_0$ | cosine of the solar zenith angle in the water |
| $n_b$ | scattering exponent |
| OAS | optically active substance |
| PAR | photosynthetically active radiation (400–700 nm) |
| $R(0\text{-},\lambda)$ | irradiance reflectance just beneath the water surface |
| $S_{\text{cdom}}$ | slope factor of CDOM absorption ($nm^{-1}$) |
| $S_{\text{Tri}}$ | slope factor of tripton absorption ($nm^{-1}$) |
| SIOP | specific inherent optical property |
| Turb | turbidity (FNU) |
| $z$ | water depth (m) |
| $Z_{\text{att}}(\lambda)$ | attenuation depth (m) |
| $Z_{\text{SD}}$ | Secchi depth (m) |



## Introduction

Subsurface reflectance and diffuse attenuation coefficient are important optical properties in the monitoring and management of surface waters. The subsurface reflectance spectrum, $R(\lambda)$, of water contains information on the concentrations of optically active substances (OAS). Consequently, monitoring of water quality by remote sensing is based on analysing the magnitude and shape of the reflectance spectrum. Before the interpretation of water quality, the satellite or airborne remote sensing measurements are usually converted into underwater reflectances after correction for atmospheric disturbance and taking into account the water/air interface (e.g. Doerffer and Fischer 1993). The most important OAS that affect light attenuation and reflectance are coloured dissolved organic matter (CDOM, i.e. humic substances), particles (phytoplankton, inorganic particles and detritus), phytoplankton pigments and pure water.

The spectral diffuse attenuation coefficient, $K_d(\lambda)$, defines the attenuation of light in the water column and thus the light availability for phytosynthesis at different depths. $K_d(\lambda)$ is needed in studying phytoplankton succession, in phytoplankton simulations in ecological models and in estimating the potential appearance depths of submerged macrophytes and periphyton, which depend on the availability of photosynthetic active radiation (PAR) and on its spectral distribution. Furthermore, $K_d(\lambda)$ is an important variable in hydrodynamic models that simulate water temperature and stratification (Huttula *et al.* 1992; Umgiesser *et al.* 2002). The determination of $K_d(\lambda)$ in the field requires suitable irradiance spectroradiometers and is laborious to measure. Therefore, a tool that could be used to calculate $K_d(\lambda)$ from the water quality measurements included in monitoring programmes would be valuable. In the routine monitoring of lakes, water transparency is often approximated by Secchi depth ($Z_{\text{SD}}$), which is simple to measure and is the only measurement offering long time series of the optical properties of surface waters. $Z_{\text{SD}}$ is also easily understandable for the public, who view water from ashore or from a boat.

$K_d(\lambda)$, $Z_{\text{SD}}$ and $R(\lambda)$ are apparent optical properties (AOPs), which depend on the inherent optical properties (IOPs, e.g. absorption, scattering and backscattering coefficients) and on the spatial distribution of the incident radiation (mainly affected by solar altitude and cloudiness). The relationships between AOPs and IOPs have been intensively studied in water optics.

Simple models, based on the IOPs, have been presented both for $K_d(\lambda)$ (e.g. Kirk 1994) and $Z_{SD}$ (Tyler 1968; Holmes 1970). Most of them were originally developed for ocean conditions. These models have also been applied in lakes in order to estimate the contribution of different OAS to $K_d(\lambda)$ and $Z_{SD}$ (Vant and Davies-Colley 1984; Bukata *et al.* 1988; Effler and Perkins 1996; Jassby *et al.* 1999; Effler *et al.* 2001, 2002; Van Duin *et al.* 2001). Furthermore, optical models are valuable tools when comparing different lake management alternatives. For example, Effler *et al.* (2001) used a simple $Z_{SD}$ model to estimate the contribution to tripton (non-living particulate matter) and chlorophyll *a* to $Z_{SD}$ in order to determine correct abatement measures (erosion vs. nutrient control) for improving lake water transparency. The attenuation properties also provide important information for remote sensing applications, as they can be used in estimating the water depth zones and locations where the remotely sensed signal is possibly influenced by reflection from the bottom.

A widely used tool in remote sensing is the bio-optical reflectance model, in which subsurface reflectance is related to total absorption and backscattering coefficients (e.g. Gordon *et al.* 1975). Absorption and backscattering coefficients are usually calculated by multiplying the OAS concentrations by the specific inherent optical properties (SIOPs), which define the absorption and backscattering coefficients per mass concentration of OAS. Such models can be applied in estimating the variability of reflectance based on typical OAS in a certain region, sensitivity analyses, estimating the applicability of current and future satellite sensors for water quality monitoring, and interpretation of OAS from measured spectra by inversion (e.g. Morel 1988). Bio-optical reflectance models have been widely used in remote sensing of lake water quality (Bukata *et al.* 1979; Dekker 1993; Hoogenboom *et al.* 1998; Podznyakov *et al.* 1998; Pierson and Strömbeck 2001; Kallio *et al.* 2005). In Finland, the number of lakes is high (56 000 larger than 0.01 $km^2$) and only a small proportion of them can be monitored annually. For example, in 2002 water samples were collected from 3589 stations representing 2111 lakes. Routine monitoring is mainly based on the collection of water samples for transportation to laboratories for further analyses. Consequently, remote sensing is a potential tool for lake monitoring in Finland. The research results from airborne and satellite remote sensing in Finnish lakes have been presented in several papers (Härmä *et al.* 2001; Kallio *et al.* 2001; Koponen *et al.* 2001; Pulliainen *et al.* 2001; Kallio *et al.* 2003; Kutser *et al.* 2005). These investigations have concentrated on a few lakes or on a specific region. For nationwide remote sensing applications, knowledge of the typical variation in $R(\lambda)$ and attenuation properties would be valuable.

Wide surveys of optical properties of lakes are rare. Rijkeboer *et al.* (1998) measured optical properties in more than 120 locations in the Netherlands covering lakes, rivers and tidal waters. The survey included radiance and Secchi depth measurements in the field, and determination of absorption spectra (phytoplankton, tripton, CDOM) and OAS concentrations (Chl-a, TSS) in the laboratory. Subsurface irradiance reflectance was calculated from the radiance measurements above the water surface. The aim of this spectral library was (1) to study the relationship between IOPs and subsurface reflectance for the purpose of remote sensing and (2) to develop an optical classification of surface waters. Rijkeboer *et al.* (1998) showed that, by using the spectral position and magnitude of the subsurface irradiance reflectance peak alone, it was possible to distinguish groups of water bodies according to morphometry and hydrology. However, the results of the cited study are not directly applicable, for example, to boreal lakes, because the number of hyper-eutrophic lakes in the Netherlands is high.

The aim of this study was to estimate $K_d(\lambda)$, attenuation depth and $R(\lambda)$ distributions for Finnish lakes. These estimations were based on the measured OAS at 1670 routine water quality monitoring stations representing 1113 lakes and on the use of simple optical models. The applied models were partly based on a bio-optical reflectance model previously

constructed for Finnish lakes. In addition, the optimum empirical water quality interpretation algorithms and the impact of CDOM variation on them were investigated on the basis of reflectance ratios using OAS concentrations typical for Finnish lakes.



## Material and methods

### Optical and limnological data

The bio-optical model which calculates the absorption and scattering coefficients, and the subsurface reflectance model needed in the analyses, were obtained from Kallio *et al.* (2005). The study by Kallio *et al.* (2005) was based on the optical investigations of the 'Satellite Remote Sensing for Lake Monitoring (SALMON)' EU project and was carried out in May and July–August in 1997–1998 in six lakes in southern Finland and five lakes in northern Finland. In the present study, this SALMON dataset (Table 1) was used for the parameterization and testing of the $K_d(\lambda)$ and $Z_{SD}$ models.

The OAS and $Z_{SD}$ data used in this study consisted of the results from national and regional monitoring carried out by regional environment centres, and by local statutory monitoring conducted by private companies and water protection associations. The Research Laboratory of the Finnish Environment Institute is the national reference laboratory, which controls the quality of the regional environment laboratories and laboratories owned by private firms or water protection associations by carrying out inter-calibration tests. At present, about 80% of the water laboratories in Finland have their methods accredited by European standards (EN ISO/IEC 17025:1999).

The nationwide data was obtained from the Environmental Information System of the Finnish Environment Administration and covered the years 2000–2002. Only results from the period July–August were accepted. This is the most important monitoring period during ice-free conditions in Finland, due to the high phytoplankton biomass, the occurrence of cyanobacteria and the low oxygen concentrations in the hypolimnion. Only those stations where all OAS (chlorophyll *a*, turbidity, water colour) and $Z_{SD}$ were measured simultaneously were accepted for the subsequent analyses. This dataset,

**Table 1** OAS concentrations and $Z_{SD}$ of the SALMON stations measured in 1997–1998. All values are based on single measurements. The stations used for the $Z_{SD}$ and $K_d(\lambda)$ model calibration/validation are indicated in the last column

| Station | Lake | Month | $C_{TSS}$ (mg l$^{-1}$) | $C_{Chl\text{-}a}$ (µg l$^{-1}$) | $a_{cdom}(400)$ (m$^{-1}$) | $Z_{SD}$ (m) | Model |
|---|---|---|---|---|---|---|---|
| Puu-m | Puujärvi | 5 | 1.9 | 4.5 | 2.1 | 3.9 | $Z_{SD}$, $K_d$ |
| Loh1-a | Lohjanjärvi | 8 | 15.5 | 55 | 5.3 | 0.8 | $Z_{SD}$ |
| Loh2-a | Lohjanjärvi | 8 | 4.6 | 13.5 | 3.8 | 1.5 | $Z_{SD}$, $K_d$ |
| Loh3-a | Lohjanjärvi | 8 | 5.9 | 10.5 | 3.9 | 1.9 | $Z_{SD}$, $K_d$ |
| Loh4-a | Lohjanjärvi | 8 | 3.0 | 11.5 | 3.3 | 2.9 | $Z_{SD}$, $K_d$ |
| Ena-a | Enäjärvi | 8 | 10 | 37 | 1.9 | 1.1 | $Z_{SD}$, $K_d$ |
| Nor1-a | Norvajärvi | 8 | 0.8 | 3.5 | 3.1 | 4.0 | $Z_{SD}$ |
| Nor2-a | Norvajärvi | 8 | 1.1 | 3.3 | 3.6 | 3.3 | $Z_{SD}$, $K_d$ |
| Sie-a | Sierijärvi | 8 | 19.6 | 73 | 18.2 | 0.4 | $Z_{SD}$, $K_d$ |
| Son-a | Sonkajärvi | 8 | 1.7 | 5.7 | 13.0 | 2.2 | $Z_{SD}$, $K_d$ |
| Poy-a | Pöyliönjärvi | 8 | 1.0 | 7.6 | 10.0 | 2.5 | $Z_{SD}$, $K_d$ |
| Vas-a | Vasikkajärvi | 8 | 0.4 | 0.8 | 0.3 | 11.8 | $Z_{SD}$ |
| Ves-a | Vesijärvi | 8 | 2 | 11.5 | 1.4 | 2.8 | $Z_{SD}$ |
| Paa1-a | Pääjärvi | 8 | 2.1 | 5.5 | 7.4 | 2.7 | $Z_{SD}$, $K_d$ |
| Paa2-a | Pääjärvi | 8 | 1.6 | 6.8 | 7.2 | 2.7 | $Z_{SD}$ |

**Table 2** Statistical characteristics of the nationwide dataset ($N = 3549$) with 10% and 90% percentiles. $C_{TSS}$ was estimated from turbidity

| | P10 | Median | P90 | Mean | Min | Max |
|---|---|---|---|---|---|---|
| $C_{TSS}$ (mg l$^{-1}$) | 0.7 | 2.20 | 9.3 | 4.3 | 0.19 | 151 |
| $C_{Chl\text{-}a}$ ($\mu$g l$^{-1}$) | 2.8 | 9.8 | 41.2 | 18.3 | 0.5 | 450 |
| $a_{cdom}(400)$ (m$^{-1}$) | 2.1 | 7.4 | 19 | 8.9 | 0.6 | 74 |
| $Z_{SD}$ (m) | 0.75 | 1.8 | 4.0 | 2.1 | 0.1 | 11 |



consisting of 3549 observations (Table 2) from 1670 stations representing 1113 lakes, was used to:

(1) simulate $R(\lambda)$ (using 3549 OAS observations).
(2) calculate $K_d$(PAR) and attenuation depth distribution (using mean OAS for 1670 stations). The station-averaged OAS represent the general OAS distributions better than the whole dataset, in which the intensively monitored stations have a greater impact than the less frequently monitored stations.
(3) calculate OAS and $Z_{SD}$ distributions of Finnish lakes according to lake size classes (using mean OAS for 1113 lakes).

#### Determination methods

In routine water quality monitoring in Finland, the concentration of humic substances is indirectly determined by the 'water colour' (mgPt l$^{-1}$) method, which is based on the comparison of water samples with standard cobalt chloride disks (EN ISO 7887:1994). The colour values are expressed as mgPt l$^{-1}$, because comparison was previously made with standard solutions of chloroplatinate ion tinted with cobalt. Turbidity (Turb, FNU units) was determined by the Nephelometric method (EN 27027:1994), based on the measurement of light (860 nm) scattered within a 90° angle from a beam directed at the water sample, using formazine as a standard matching solution. The concentration of total suspended solids ($C_{TSS}$) was measured using gravimetric determination of the matter removed by a filter (EN 872:1996, Nuclepore polycarbonate 0.4 $\mu$m filter). The sum of chlorophyll *a* and phaeophytin *a* ($C_{Chl\text{-}a}$) was determined with a spectrophotometer after extraction with hot ethanol (ISO 10260:1992, GF/C filter). $Z_{SD}$ was measured using the white top (diameter about 12 cm) of the water sampler. The OAS concentrations were determined from water samples taken at a depth of 1 m with the exception of $C_{Chl\text{-}a}$ (composite sample of 0–2 m).

The bio-optical model used to calculate the total absorption coefficient, total scattering coefficient and reflectance requires $C_{TSS}$, absorption coefficient of CDOM at 400 nm ($a_{cdom}(400)$) and $C_{Chl\text{-}a}$ as inputs (Kallio *et al.* 2005). Because $C_{TSS}$ and $a_{cdom}(400)$ were measured at only a few stations in the national dataset, $C_{TSS}$ was here estimated from turbidity and $a_{cdom}(400)$ from Pt water colour. $a_{cdom}(400)$ was derived from: $a_{cdom}(400) = 0.123 \times$ colour ($R^2 = 0.832$, $n = 449$, $a_{cdom}(400)$ range: 0.1–34 m$^{-1}$). This relationship was based on data in the Environmental Information System (July–August observations in 2000–2002, $N = 388$) and from the airborne spectrometer measurement campaigns (July–August observations in 1997–1998, $N = 61$). All $a_{cdom}(400)$ were measured from a depth of 1 m. $C_{TSS}$ was estimated from $C_{TSS} = 1.162 \times$ Turb ($R^2 = 0.815$, $N = 106$, $C_{TSS}$ range: 0.4–17 mg l$^{-1}$). This relationship was obtained using the same data sources as in the case of $a_{cdom}(400)$ estimation. The correlations between the four variables

($C_{TSS}$, $C_{Chl\text{-}a}$, Pt water colour, $Z_{SD}$) in the whole dataset ($N = 3549$) were low($R < 0.48$) with the exception of Turb vs $C_{Chl\text{-}a}$ ($R = 0.64$) and Pt water colour vs $Z_{SD}$ ($R = -0.57$).

#### Optical models

*Bio-optical model*. The bio-optical model has previously been tested using the SALMON optical dataset (Kallio *et al.* 2005). The total absorption ($a_{Tot}(\lambda)$) and scattering ($b_{Tot}(\lambda)$) coefficients are calculated in the model from SIOPs and OAS concentrations and they form the basis of the $Z_{SD}$ and $K_d$ models of this study. Furthermore, the bio-optical model estimates the backscattering coefficient ($b_{b,Tot}(\lambda)$), that enables calculation of the subsurface irradiance reflectance spectrum $R(\lambda)$. The models simulate optical properties in the 400–750 nm range with a step of 2 nm. The statistical accuracy characteristics of the bio-optical model have been described in Kallio *et al.* (2005). In the case of reflectance $R^2$ was 0.921 and rmse was 24.8%, when tested using the 12 SALMON stations. The greatest discrepancies were in the three eutrophic lakes, probably due to the variation in absorption and backscattering properties of phytoplankton.

Four optically active components are assumed in the model: phytoplankton, tripton, coloured dissolved organic matter and pure water. The total spectral absorption coefficient ($a_{Tot}(\lambda)$) is described by

$$a_{Tot}(\lambda) = a_w(\lambda) + a_{cdom}(\lambda) + a_{Ph}(\lambda) + a_{Tri}(\lambda) \quad (1)$$

where $a_w(\lambda)$ is the absorption coefficient of pure water (Buiteveld *et al.* 1994), $a_{ph}(\lambda)$ is the absorption coefficient of phytoplankton, $a_{cdom}(\lambda)$ is the absorption coefficient of CDOM and $a_{Tri}(\lambda)$ is the specific absorption coefficient of tripton.

Absorption by CDOM is calculated by assuming an exponential increase with a decreasing wavelength (Bricaud *et al.* 1981):

$$a_{cdom}(\lambda) = a_{cdom}(400)e^{-S_{cdom}(\lambda-400)} \quad (2)$$

where $a_{cdom}(400)$ is the absorption coefficient of CDOM at 400 nm and $S_{cdom}$ is the slope factor.

Absorption by phytoplankton, $a_{ph}(\lambda)$, is calculated by

$$a_{Ph}(\lambda) = a^*_{ph}(\lambda)C_{Chl-a} \quad (3)$$

where $a^*_{ph}(\lambda)$ is the Chl-*a* specific absorption coefficient of phytoplankton. $a^*_{ph}(\lambda)$, decreases in the model with increasing $C_{Chl\text{-}a}$ according to measurements made in Finnish lakes (Ylöstalo *et al.* 2005).

Absorption by tripton, $a_{Tri}(\lambda)$, is expressed as

$$a_{Tri}(\lambda) = a^*_{\underline{TSS}}(\lambda)C_{TSS} \quad (4)$$

where $a^*_{\underline{TSS}}(\lambda)$ is the specific absorption of bleached total suspended solids and $C_{TSS}$ is the concentration of TSS. Absorption by tripton is defined using $C_{TSS}$, because tripton concentration measurements were not available. $a^*_{\underline{TSS}}(\lambda)$ is described analogously to the calculation of $a_{cdom}(\lambda)$ (Roesler *et al.* 1989):

$$a^*_{\underline{TSS}}(\lambda) = a^*_{\underline{TSS}}(400)e^{-S_{Tri}(\lambda-400)} \quad (5)$$

where $a^*_{\underline{TSS}}(400)$ is the specific absorption of bleached total suspended solids at 400 nm and $S_{Tri}$ is the slope factor of tripton absorption.

The total scattering coefficient, $b_{tot}(\lambda)$, is described by

$$b_{tot}(\lambda) = b_w(\lambda) + b^*_{TSS}(\lambda)C_{TSS} \quad (6)$$

where $b_w$ is the scattering coefficient of pure water (Buiteveld *et al.* 1994), and $b^*_{TSS}$ is the specific scattering coefficient of TSS.

The specific scattering coefficient of TSS ($b^*_{TSS}(\lambda)$) is described by a power function (e.g. Maffione and Dana 1996; Herlevi 2002):

$$b^*_{TSS}(\lambda) = b^*_{TSS}(555)\left(\frac{555}{\lambda}\right)^{n_b} \quad (7)$$

where $b^*_{TSS}(555)$ is the specific scattering coefficient of TSS at 555 nm and $n_b$ is the scattering exponent.

The total attenuation coefficient is the sum of the absorption and scattering coefficients:

$$c_{Tot}(\lambda) = a_{Tot}(\lambda) + b_{Tot}(\lambda). \quad (8)$$

The total backscattering coefficient, $b_{b,tot}(\lambda)$, needed in the reflectance model, is described by

$$b_{b,}\mathrm{tot}(\lambda) = bp_w b_w(\lambda) + bp_{TSS} b^*_{TSS}(\lambda) C_{TSS} \quad (9)$$

where $b_w$ is the scattering coefficient of pure water and $b^*_{TSS}$ is the specific scattering coefficient of TSS. $bp_w$ and $bp_{TSS}$ are the backscattering ratios of pure water and TSS, respectively. The coefficients of the bio-optical model are summarized in Table 3.

*Reflectance model*. Calculation of irradiance reflectance just beneath the water surface, $R(0\text{-},\lambda)$, is based on the following equation (Gordon *et al.* 1975; simplified by Jerlov 1976):

$$R(0-,\lambda) = C\frac{b_{b,Tot}(\lambda)}{a_{Tot}(\lambda) + b_{b,Tot}(\lambda)} \quad (10)$$

where $b_{b,Tot}(\lambda)$ is the total backscattering coefficient and $a_{Tot}(\lambda)$ is the total absorption coefficient. The coefficient $C$ depends mainly on the illumination and the viewing geometry. $C$ is estimated by the equation presented by Kirk (1984a):

$$C = -0.629\mu_0 + 0.975 \quad (11)$$

where $\mu_0$ is the cosine of the solar zenith angle in the water. The solar zenith angle used in all $R(\lambda)$ calculations was 46.3° (1 August, 13.00 local time, latitude 64°N). $a_{Tot}(\lambda)$ and $b_{b,Tot}(\lambda)$ are obtained by summing up the absorption and backscattering coefficients of the optically active substances in the water (Equations (1) and (9)).

*Diffuse attenuation coefficient and Secchi depth models*. The simple $Z_{SD}$ and $K_d(\lambda)$ models were parameterized using the optical dataset from the SALMON project. This dataset

**Table 3** Coefficients of the bio-optical reflectance model

| Coefficient | Symbol | Value | Source |
|---|---|---|---|
| Absorption coefficient of pure water | $a_w(\lambda)$ | See the reference | Buiteveld *et al.* (1994) |
| Specific absorption of phytoplankton | $a^*_{ph}(\lambda)$ | See the reference | Ylöstalo *et al.* (2005) |
| Slope factor of CDOM absorption | $S_{CDOM}$ | 0.0150 $nm^{-1}$ | Kallio *et al.* (2005) |
| Specific absorption of bleached TSS at 400 nm | $a^*_{TSS}(400)$ | 0.13 l $m^{-1}mg^{-1}$ | Ylöstalo *et al.* (2005) |
| Slope factor of tripton absorption | $S_{tri}$ | 0.012 $nm^{-1}$ | Ylöstalo *et al.* (2005) |
| Specific scattering of TSS at 555 nm | $b^*_{TSS}(555)$ | 0.811 l $m^{-1}mg^{-1}$ | Kallio *et al.* (2005) |
| Scattering exponent of TSS | $n_b$ | 0.705 | Kallio *et al.* (2005) |
| Scattering coefficient of pure water | $b_w(\lambda)$ | See the reference | Buiteveld *et al.* (1994) |
| Backscattering probability of pure water | $bp_w$ | 0.5 | Sathyendranath *et al.* (1989) |
| Backscattering probability of TSS | $bp_{TSS}$ | 0.0131 | Kallio *et al.* (2005) |

consisted of underwater irradiance (Li1800UW), absorption and scattering coefficients (ac-9 absorption/attenuation meter), OAS and $Z_{SD}$ measurements in 10 lakes (Table 1). Two simple $K_d$ models were tested, in which $K_d(\lambda)$ is calculated from the absorption and scattering coefficients. The following model is based on the work of, for example, Maffione and Jaffe (1995) and has previously been used in Finnish and Estonian lakes by Herlevi (2002):

$$K_d(\lambda) = D_1 a(\lambda) + D_2 b(\lambda) \tag{12}$$

where $D_1$ and $D_2$ are empirical coefficients.

Kirk's (1984b) model for the mean $K_d(\lambda)$ in the euphotic zone also takes into account the solar altitude dependence

$$K_d(\lambda) = \frac{1}{u_0}(a(\lambda)^2 + (g_1 u_0 - g_2) b(\lambda) a(\lambda))^{1/2} \tag{13}$$

where $u_0$ is the cosine of the solar zenith angle in the water. Coefficients $g_1$ and $g_2$ depend on the shape of the scattering phase function. Here $g_1 = 0.425$ and $g_2 = 0.190$ were used as proposed by Kirk (1984b).

The spectral diffuse attenuation coefficient $K_d(\lambda)$ needed in the model calibration was calculated from the downwelling irradiances ($E_d(\lambda)$) measured by the Li1800UW underwater spectrometer:

$$K_d(\lambda) = \frac{1}{z_2 - z_1} \ln \left[ \frac{E_{d,z_1}(\lambda)}{E_{d,z_2}(\lambda)} \right] \tag{14}$$

where $z_1$ is 0.5 m and $z_2$ is 1.0 m water depth.

The attenuation depth $z_{att}(\lambda)$ was calculated by

$$z_{att}(\lambda) = \frac{1}{K_d(\lambda)} \tag{15}$$

The first simple $Z_{SD}$ model applied here was presented by Höjerslev (1986, see Preisendorfer 1986):

$$Z_{SD} = C_1 \frac{1}{c_{Tot}(\mathrm{PAR})} \tag{16}$$

where $C_1$ is an empirical coefficient and $c_{Tot}(\mathrm{PAR})$ is the total beam attenuation coefficient of the PAR (400–700 nm) region.

The second model, presented by Tyler (1968), relates $Z_{SD}$ to the sum of $c_{Tot}(\mathrm{PAR})$ and $K_d(\mathrm{PAR})$:

$$Z_{SD} = C_2 \frac{1}{c_{Tot}(\mathrm{PAR}) + K_d(\mathrm{PAR})} \tag{17}$$

where $C_2$ is an empirical coefficient and $K_d(\mathrm{PAR})$ is the diffuse attenuation coefficient of PAR.

The accuracy characteristics of the models were defined by $R^2$ and root mean squared error (rmse), which is defined as

$$\mathrm{rmse} = \sqrt{\frac{1}{N-2} \sum_{i=1}^{N} (\hat{Y}_i - Y_i)^2} \tag{18}$$

where $\hat{Y}_i$ is the estimated value, $Y_i$ is the measured value and $N$ is the total number of

observations. The relative rmse (%) was calculated from the rmse and the mean measured value.

## Results and discussion

### Diffuse attenuation coefficient and Secchi depth models

The $K_d$ model (Equation (12)) was calibrated against the measured $K_d(\lambda)$ of the SALMON optical dataset, which resulted in $D_1 = 1.123$ and $D_2 = 0.142$ (Figure 1). The rmse of the different stations ranged between 9.7 and 21.0% (mean 15.8%) and $R^2$ between 0.94 and 0.99. The $K_d$ model using the empirical coefficients ($D_1 = 1.21$ and $D_2 = 0.19$) reported by Herlevi (2002) for Finnish and Estonian lakes yielded higher $K_d$ (rmse 11.2–30.6, mean 21.2%, see Figure 1) than the calibrated $D_1$ and $D_2$ of this study. One reason for the differences may be the fact that Herlevi (2002) used measured $a$ and $b$ (with ac-9 absorption/attenuation meter) at nine wavelengths (412, 440, 488, 510, 532, 555, 650, 676 and 715 nm) in the model, whereas here the $K_d$ model was based on the full spectral $a_{Tot}$ and $b_{Tot}$ (with 2 nm step) obtained from the bio-optical model. Only seven stations could be used in the calibration, because in other stations the measured $K_d(\lambda)$ was noisy or not reliable due to the high attenuation of radiation, which resulted in low irradiance levels, particularly at a depth of 1 m. However, $K_d$ of three of the excluded stations was reliable for the greater part of the

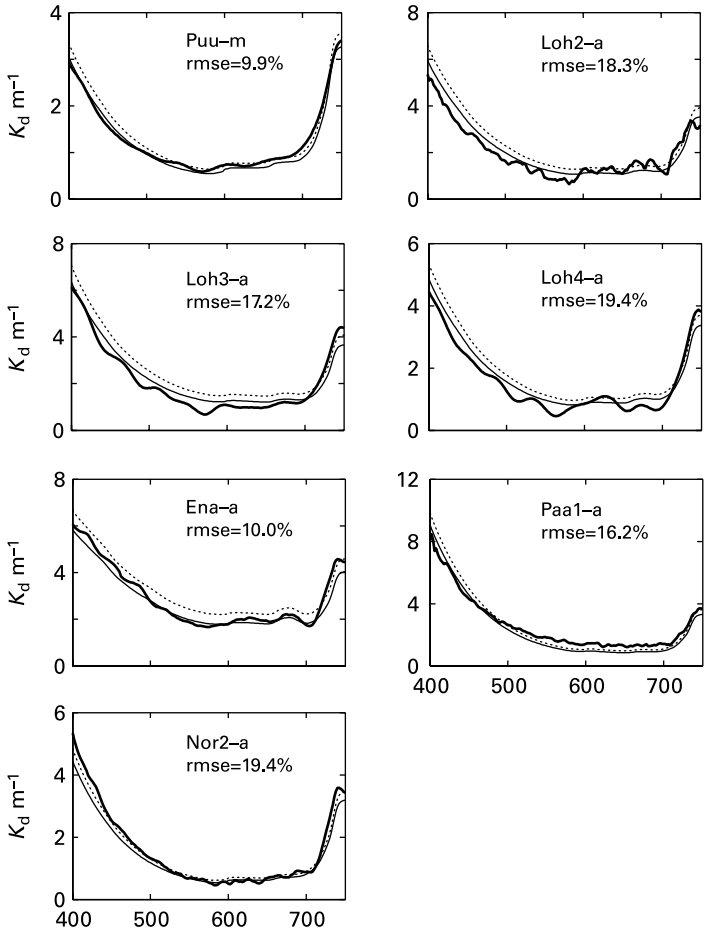


**Figure 1** Measured (—) and simulated (—) attenuation coefficient ($K_d(\lambda)$) in the SALMON stations used in calibration of the $K_d(\lambda)$ model (Equation (12)). The simulated $K_d(\lambda)$ (···) using the coefficients of Herlevi (2002) are also shown

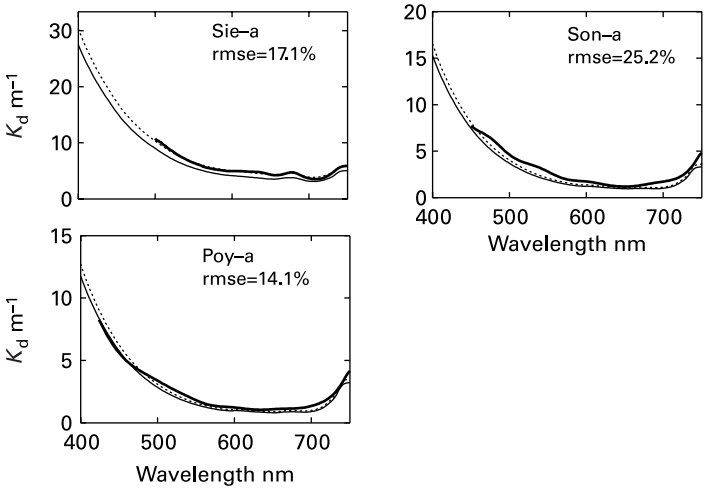


**Figure 2** Measured (—) and simulated (—) attenuation coefficient ($K_d(\lambda)$) in the SALMON stations used in the validation of the $K_d(\lambda)$ model (Equation (12)). The simulated $K_d(\lambda)$ (···) using the coefficients of Herlevi (2002) are also shown

spectrum and these stations were used for validation of the model (Figure 2). The simulated $K_d(\lambda)$ of the three validation stations were slightly lower than the measured values (rmse between 14.1 and 25.3%). Here, the coefficients reported by Herlevi (2002) yielded smaller rmse (3.6–17.1%) than the calibrated coefficients of the present study. However, the validation accuracy characteristics are not directly comparable with those of the calibration results, because of the lack of measured $K_d(\lambda)$ at short wavelengths. Herlevi (2002) calibrated the model separately for humic lakes and obtained $D_1 = 1.15$ and $D_2 = 0.38$. The number of lakes in the SALMON dataset used here was so low that a separate analysis by lake type was not possible.

The test of the $K_d$ model (Equation (13)) with fixed $g_1$ and $g_2$ (Kirk 1984b) and sun elevation dependency resulted in a slightly higher rmse (11.9–22%, mean 17.7%) than Equation (12), when compared with the measured $K_d$ of the calibration stations. Because Equation (12) is simpler to apply than Equation (13) and the statistical performance of the two equations was about the same, Equation (12) was used in the further calculation of nationwide distributions of $K_d$ and $Z_{att}$.

The $Z_{SD}$ model (Equation (16)) was tested using 14 measurements of the SALMON dataset. The attenuation coefficient in the 400–700 nm (PAR) region was calculated by: $c_{Tot}(PAR) = a_{Tot}(PAR) + b_{Tot}(PAR)$, where $a_{Tot}(PAR)$ and $b_{Tot}(PAR)$ were obtained from Equations (1) and (6). The correlation between $c_{Tot}(PAR)$ and $Z_{SD}$ is presented in Figure 3. The calibration of the model (Equation (16)) resulted in $C_1 = 7.26$ ($R^2 = 0.965$, rmse = 18.5%, $N = 14$). The exclusion of the highest $Z_{SD}$ (11.5 m) decreased $R^2$ to 0.74, but $C_1$ (7.46) changed only slightly. The calibration of the other model (Equation (17)) resulted in $Z_{SD} = 11.4/(c_{Tot}(PAR) + K_d(PAR))$ with almost the same accuracy ($R^2 = 0.960$ and rmse = 19.8%) as Equation (12). $K_d(PAR)$ in Equation (13) was calculated by the $K_d(\lambda)$ model (Equation (12)), because measured $K_d(\lambda)$ was not available from all SALMON stations.

Herlevi (2002) investigated the relationship between $Z_{SD}$ and $c_{Tot}(PAR)$ in Finnish and Estonian lakes using the same equation as in this study (Equation (16)). Herlevi (2002), who estimated $c_{Tot}(PAR)$ from $c$ measured with the ac-9 instrument at 9 wavelengths, reported $Z_{SD} = 8.4/c_{Tot}(PAR)$ ($R^2 = 0.94$, $N = 66$) and thus obtained a slightly higher $C_1$ than that obtained in this study (7.26). The empirical coefficient ($C_2 = 11.4$) of the other $Z_{SD}$ model

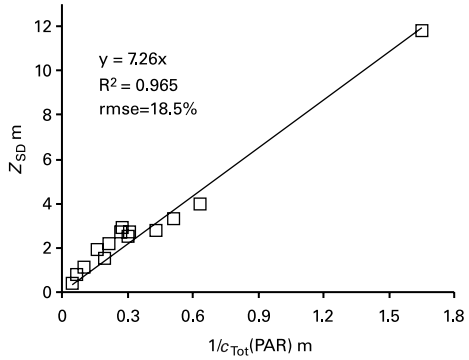


**Figure 3** Correlation between measured Secchi depth ($Z_{SD}$) and $1/c_{Tot}$(PAR) in the SALMON dataset ($N = 14$)

(Equation (17)) was close to that reported by Herlevi (2002) ($C_2 = 11.2$, $N = 66$, $R^2 = 0.93$). These $C_2$ values (Equation (17)) are higher than those obtained in oceanic and coastal waters; for example Tyler (1968) reported $C_2 = 8.69$ ($Z_{SD}$ range 10–48 m) and Holmes (1970) $C_2 = 9.42$ ($Z_{SD}$ range 2–12 m). Davies-Colley (1988) found $C_2 = 9.52$ ($Z_{SD}$ range 0.42–17.7 m) for lakes in New Zealand. $Z_{SD}$ is an apparent optical property which depends, for example, on the incident light field (solar angle, cloudiness), the surface roughness of the water (if an underwater viewer is not used) and the reflectance of the disk. Preisendorfer (1986) presented detailed equations of the factors affecting $Z_{SD}$, but its precise modeling is difficult.

Another type of simple optical model is based on the calculation of $Z_{SD}$ and $K_d$(PAR) directly from the OAS concentrations using multiple regression (e.g. Reinart *et al.* 2001; Van Duin *et al.* 2001). The models in the present study are based on the calculation of $a_{Tot}(\lambda)$ and $b_{Tot}(\lambda)$ and they are more potential tools for, for example, lake management than the purely empirical models. This is because case-specific SIOPs and non-linear relationships (e.g. package effect of phytoplankton absorption) at different OAS concentrations can be taken into account.

#### Frequency distributions

The cumulative frequency distributions of the measured OAS and $Z_{SD}$ for all lakes, small lakes ($< 0.5\,km^2$) and large lakes ($> 100\,km^2$) are presented in Figure 4. The frequencies were calculated from the mean OAS for each lake, and lake areas were obtained from the Lake Register of the Environmental Information System maintained by the Finnish Environmental Administration. The OAS concentrations in large lakes are clearly lower than in the whole dataset (all lakes), whereas in small lakes the concentrations are only slightly higher. Although the number of large lakes in Finland is low (46 lakes $> 100\,km^2$, the present study included 44 of them), they represent 43.5% of the total lake area (32 333 $km^2$) in Finland (Raatikainen and Kuusisto 1990). The share of small lakes ($< 0.05\,km^2$) is only 0.2% of the total lake area.

The spectral $K_d$ for the stations of the national dataset were calculated using Equation (12). $a_{tot}$ and $b_{tot}$ for each station were calculated by the bio-optical model using the station averaged OAS ($N = 1670$). The cumulative frequency distribution of $K_d$(PAR) is presented in Figure 5(a). The mean $K_d$(PAR) was $3.5\,m^{-1}$ and median $2.8\,m^{-1}$ (Table 4). The spectral attenuation depths, $Z_{att}(\lambda)$, were calculated from the simulated $K_d(\lambda)$ (Equation (15)). The cumulative frequencies of maximum $Z_{att}$ and the position of maximum $Z_{att}$ are presented in Figures 5(b) and (c). The mean of maximum $Z_{att}$ was 1.23 m and median 1.05 m (Table 4). The location of the maximum $Z_{att}(\lambda)$ (Figure 5(c)) was between 564 and 714 nm, with the

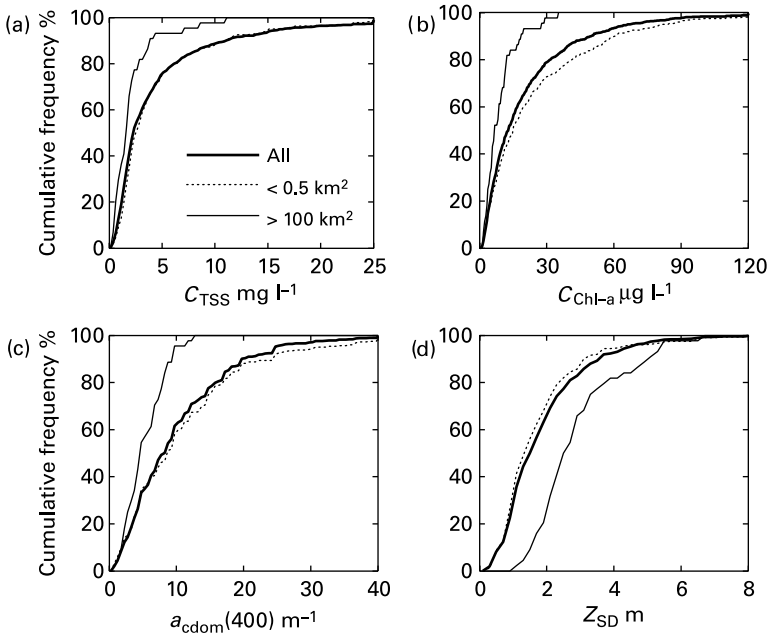


**Figure 4** Cumulative frequency distributions of OAS (Chl *a*, TSS, $a_{cdom}(400)$) and $Z_{SD}$ in the lake averaged dataset. Frequency distributions are presented for all lakes ($N = 1113$), large lakes ($N = 44$, $A > 100\,km^2$) and small lakes ($N = 321$, $A > 0.5\,km^2$). $C_{TSS}$ was estimated from turbidity

exception of the 589–648 nm region (due to the increased attenuation caused by absorption by pure water, see Figure 6) and the 655–688 nm region (phytoplankton absorption peak). At wavelengths $< 564$ nm, absorption by CDOM increases attenuation and at wavelengths $> 714$ nm, absorption by pure water increases sharply with increasing wavelength.

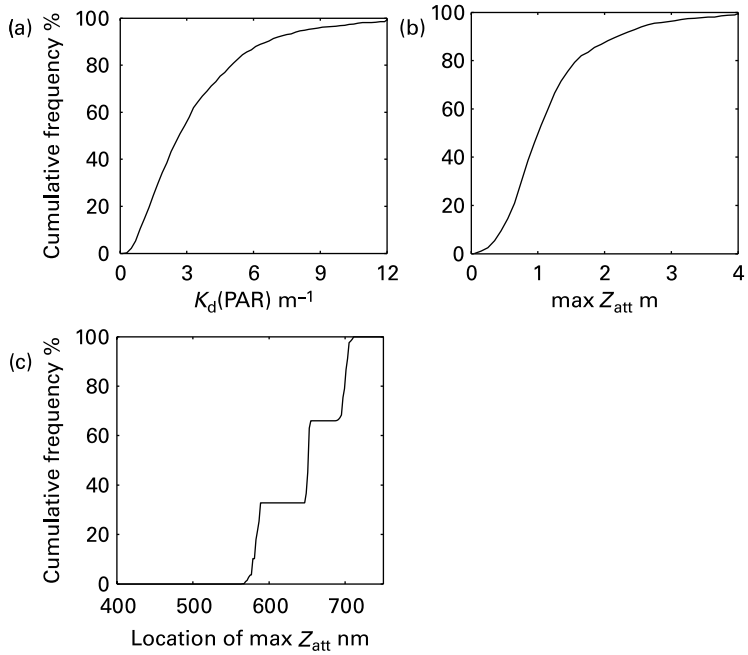


**Figure 5** Cumulative frequency diagrams of $K_d$(PAR), maximum attenuation depth (max $Z_{att}$) and the location of maximum $Z_{att}$ in the 400–750 nm range ($N = 1670$)

**Table 4** Statistical characteristics of $K_d$(PAR), max $Z_{att}$ and $Z_{att}$ at four wavelengths ($N = 1670$). P10 and P90 are the 10% and 90% percentiles

| | Units | P10 | Median | P90 | Mean | Min | Max |
|---|---|---|---|---|---|---|---|
| $K_d$(PAR) | $m^{-1}$ | 0.90 | 2.75 | 6.7 | 3.46 | 0.374 | 28.6 |
| Max $Z_{att}$ | m | 0.45 | 1.05 | 2.20 | 1.23 | 0.06 | 5.55 |
| $Z_{att}$(400) | m | 0.035 | 0.102 | 0.32 | 0.154 | 0.013 | 1.25 |
| $Z_{att}$(490) | m | 0.125 | 0.33 | 1.03 | 0.48 | 0.03 | 3.8 |
| $Z_{att}$(666) | m | 0.435 | 0.96 | 1.53 | 0.97 | 0.05 | 1.96 |
| $Z_{att}$(706) | m | 0.51 | 0.91 | 1.15 | 0.86 | 0.062 | 1.28 |



The distribution of the location of maximum $Z_{att}$ divides the lakes into three groups of approximately equal size: (1) location of max $Z_{att} < 589$ nm, (2) 589 nm < location of max $Z_{att} < 655$ nm and (3) 655 nm < location of max $Z_{att}$. The OAS concentrations increase, and $Z_{SD}$ and maximum $Z_{att}$ decrease as the location of max $Z_{att}$ moves to longer wavelengths. Thus, group 1 (mean OAS: $C_{Chl\text{-}a} = 5.8\,\mu g\,l^{-1}$, $a_{cdom}(400) = 3.1\,m^{-1}$, $C_{TSS} = 1.5\,mg\,l^{-1}$) typically consists of clear water lakes and group 3 (mean OAS $C_{Chl\text{-}a} = 46\,\mu g\,l^{1}$, $a_{cdom}(400) = 18.2\,m^{-1}$, $C_{TSS} = 11.6\,mg\,l^{-1}$) of eutrophic and hyper-eutrophic lakes.

The frequency distributions of $Z_{att}$ were also examined at those wavelengths (490, 666 and 706 nm, see Figure 7) which provide the basis for the empirical remote sensing algorithms. The reflectances or reflectance ratios of these wavelengths have proved to be the best for estimations of $C_{TSS}$ (R(706)), $C_{Chl\text{-}a}$ (ratio $R(706)/R(666)$) and $a_{cdom}(400)$ (ratio $R(666)/R(490)$) in Finnish lakes, as indicated by airborne remote sensing and subsurface reflectance measurements (Kallio *et al.* 2001, 2005). In order to show the high attenuation of blue light due to high CDOM concentrations typical for Finnish lakes, $Z_{att}(400)$ is also presented in Figure 7. The behaviour of $Z_{att}$ at different wavelengths is mainly explained by differences in the absorption spectra. At 490 nm, $Z_{att}$ is strongly influenced by $a_{cdom}$, whereas at 666 nm $Z_{att}$ is mainly affected by $a_{ph}$ and $a_w$ (Figure 6). At 706 nm, absorption is dominated by pure water. Scattering increases attenuation throughout the spectrum and depends only slightly on wavelength (it is assumed in the bio-optical model that scattering decreases slightly with increasing wavelength).

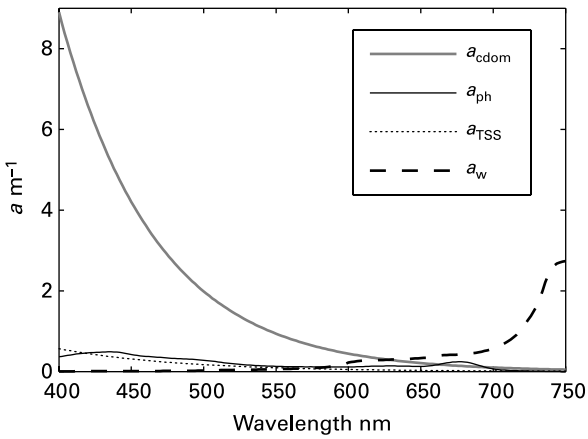


**Figure 6** Absorption spectra of the main absorbing OAS and pure water. The spectra were calculated by the bio-optical model using the mean OAS ($C_{Chl\text{-}a} = 18.3\,\mu g\,l^{-1}$, $C_{TSS} = 4.3\,mg\,l^{-1}$, $a_{cdom}(400) = 8.9\,m^{-1}$) of the nationwide dataset (Table 2)

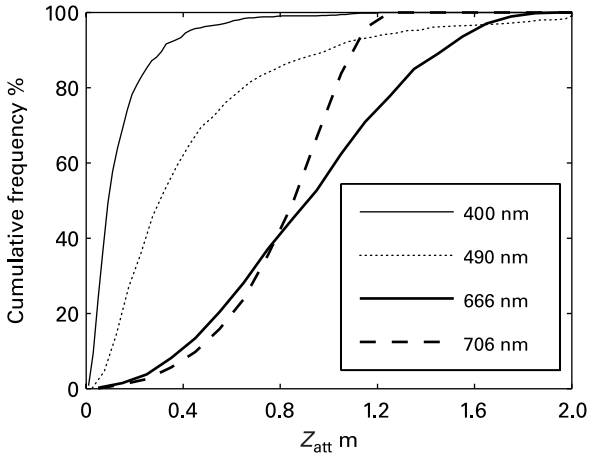


**Figure 7** Cumulative frequency diagrams of attenuation depth ($Z_{att}$) at 400, 490, 666 and 706 nm ($N = 1670$)

The attenuation depth $Z_{att}$ has two applications in the remote sensing of water quality. Firstly, $Z_{att}$ defines the depth of the surface layer represented by the remotely sensed estimates: about 90% of the backscattered light from the water to the atmosphere comes from the surface layer down to $Z_{att}$. Radiation at 666 nm penetrates deepest (Figure 7) of the wavelengths of the potential remote sensing algorithms. Therefore, $C_{Chl\text{-}a}$ and $a_{cdom}(400)$ estimations by these remote sensing algorithms are more sensitive to bottom reflection than $C_{TSS}$ estimation (using $R(706)$). Secondly, those areas where reflection from the bottom may influence the remotely sensed signal can be estimated by using $Z_{att}$ together with a bathymetric map.

#### Reflectances and empirical OAS algorithms

The typical $R(\lambda)$ of four trophic classes (simulated using the mean OAS of each trophic class) are presented in Figure 8. The location of maximum $R$ moves to longer wavelengths as the trophic status changes from oligotrophic (maximum at about 585 nm) to hyper-eutrophic (maximum at about 705 nm). The trophic classification (Table 5) is based on the maximum $C_{Chl\text{-}a}$ concentration criteria of OECD (1982): oligotrophic ($C_{Chl\text{-}a} < 8\ \mu g\ l^{1}$), mesotrophic

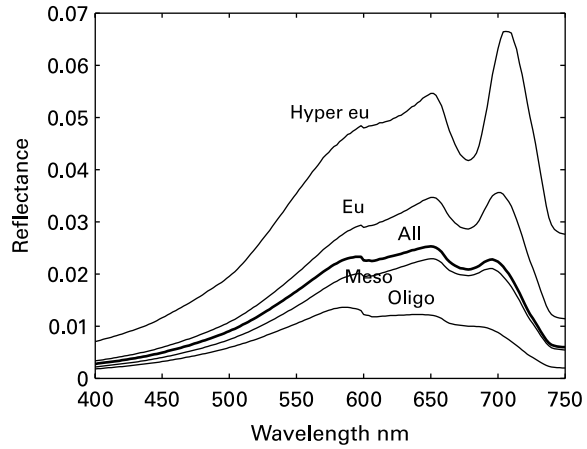


**Figure 8** Typical subsurface irradiance reflectance ($R(\lambda)$) of the four trophic classes. The spectra were calculated by the $R(\lambda)$ model using the mean OAS (Table 5) for each trophic class

**Table 5** Statistical characteristics of $C_{TSS}$, $a_{cdom}(400)$ and $Z_{SD}$ by trophic class in the nationwide dataset ($N = 3549$). P10 and P90 are the 10% and 90% percentiles. $C_{TSS}$ was estimated from turbidity

| | Oligo < 8 μg l$^{-1}$ mean = 4.5 μg l$^{-1}$ | Meso 8–25 μg l$^{-1}$ mean = 14.4 μg l$^{-1}$ | Eu 25–75 μg l$^{-1}$ mean = 39.8 μg l$^{-1}$ | Hyper >75 μg l$^{-1}$ mean = 114 μg l$^{-1}$ |
|---|---|---|---|---|
| $C_{TSS}$ | | | | |
| P10 | 0.56 | 1.51 | 2.32 | 3.14 |
| Median | 1.16 | 2.9 | 6.04 | 17.2 |
| P90 | 2.21 | 7.03 | 17.9 | 51.1 |
| Mean | 1.41 | 3.98 | 8.56 | 21.8 |
| Min | 0.2 | 0.6 | 1.2 | 0.9 |
| Max | 40 | 63 | 58 | 151 |
| $a_{cdom}(400)$ | | | | |
| P10 | 1.23 | 3.69 | 4.92 | 3.7 |
| Median | 4.31 | 8.61 | 12.3 | 12.3 |
| P90 | 9.84 | 19.7 | 24.6 | 24.6 |
| Mean | 5.07 | 10.56 | 13.8 | 13.8 |
| Min | 0.6 | 0.6 | 0.6 | 1.2 |
| Max | 67 | 73.8 | 61.5 | 49.2 |
| $Z_{SD}$ | | | | |
| P10 | 1.7 | 0.9 | 0.5 | 0.30 |
| Median | 2.9 | 1.50 | 1.00 | 0.60 |
| P90 | 5.0 | 2.7 | 1.5 | 1.5 |
| Mean | 3.15 | 1.59 | 1.00 | 0.73 |
| Min | 0.3 | 0.2 | 0.2 | 0.1 |
| Max | 11.0 | 4.2 | 3.3 | 1.8 |
| N | 1518 | 1280 | 617 | 134 |

($8\,\mu g\,l^{-1} < C_{Chl\text{-}a} < 25\,\mu g\,l^{1}$), eutrophic ($25\,\mu g\,l^{-1} < C_{Chl\text{-}a} < 75\,\mu g\,l^{-1}$), and hyper-eutrophic ($C_{Chl\text{-}a} < 75\,\mu g\,l^{-1}$).

The optimum empirical algorithms in the estimation of OAS from the reflectance spectra were investigated on the basis of the simulated $R(\lambda)$ for the whole dataset ($N = 3549$). The simulated $R(\lambda)$ were first divided into three classes according to trophic status and each class was further divided into two sub-groups: low and high CDOM levels (the threshold value was the median $a_{cdom}(400)$ of the class, Table 5). The high $C_{TSS}$ and $a_{cdom}(400)$ (> 95% percentile of each class) were excluded from the analyses, because they may include erroneous measurements. A few high concentrations have a strong impact on $R^2$ and may lead to wrong conclusions. The hyper-eutrophic ($C_{Chl\text{-}a} > 75\,\mu g\,l^{-1}$) class was not included in the analyses because of the high variation of OAS concentrations. The number of hyper-eutrophic lakes in Finland is also low (3.2% of the 1670 stations of this study were classified as hyper-eutrophic).

The simulated reflectance spectra were averaged for every 10 nm with channel centres ranging from 405 to 745 nm. Next, the correlations between all possible channel ratios (and all single channels) and OAS were calculated. $C_{TSS}$ correlated best with reflectance at > 700 nm (Table 6). In this region the absorption by other OAS (CDOM, phytoplankton) and their impact on reflectance are small. Although $R^2$ was highest at 750 nm, the 700–730 nm region is usually best for $C_{TSS}$ estimation by remote sensing (e.g. Kallio *et al.* 2001). In the 730–750 nm region, reflectance is low due to strong absorption by pure water, which leads to low reflectance. $C_{Chl\text{-}a}$ correlated best with a channel ratio of $R$ between 690 and 710 nm and $R$ between 660 and 680 nm (Table 6, Figures 9(b) and 10). This 'near-infrared (NIR)/red' ratio has often been used in lake Chl-*a* mapping (e.g. Millie *et al.* 1992; Dekker 1993; Gitelson *et al.* 1993; Schalles *et al.* 1998; Kallio *et al.* 2001, 2003; Pierson and Strömbeck 2001).

**Table 6** $R^2$ between simulated channel ratios and measured OAS. The threshold values between the low and high $a_{cdom}(400)$ sub-groups are the medians of each trophic class: 4.3 $m^{-1}$ (oligotrophic), 8.6 $m^{-1}$ (mesotrophic) and 12.3 $m^{-1}$ (eutrophic)

| OAS | Ratio | Oligotrophic | | Mesotrophic | | Eutrophic | |
|---|---|---|---|---|---|---|---|
| | | Low CDOM $N = 797$ | High CDOM $N = 506$ | Low CDOM $N = 547$ | High CDOM $N = 608$ | Low CDOM $N = 265$ | High CDOM $N = 294$ |
| $C_{Chl\text{-}a}$ | $R(705)/R(675)$ | 0.907 | 0.762 | 0.926 | 0.839 | 0.970 | 0.964 |
| | $R(695)/R(675)$ | 0.912 | 0.796 | 0.928 | 0.852 | 0.936 | 0.942 |
| | $R(705)/R(665)$ | 0.823 | 0.534 | 0.802 | 0.631 | 0.922 | 0.858 |
| | $R(695)/R(665)$ | 0.786 | 0.455 | 0.699 | 0.498 | 0.796 | 0.637 |
| $a_{cdom}$ (400) | $R(705)/R(485)$ | 0.948 | 0.969 | 0.948 | 0.992 | 0.938 | 0.993 |
| $C_{TSS}$ | $R(705)$ | 0.998 | 0.996 | 0.995 | 0.986 | 0.983 | 0.985 |

The algorithm is based on the phytoplankton absorption maximum at about 675 nm. 705 nm is good reference wavelength, because at 705 nm the impact of other absorbing OAS is small. $a_{cdom}(400)$ was best predicted by linear regression against a ratio of reflectance at wavelength $>600$ nm to reflectance in the 400–580 nm range (Table 6, Figures 9(a) and 10). This is in accordance with the findings of, for example, Pierson and Strömbeck (2000), Kallio *et al.* (2005) and Kutser *et al.* (2005). In this algorithm, the reflection changes due to CDOM absorption in the short wavelength region are normalized by changes in reflection not related to CDOM in the longer wavelengths. Correlation in the eutrophic lakes was highest if the reflectance in the numerator of the reflectance ratio was from the region 695–710 nm and 705 nm was therefore selected for the subsequent analyses.

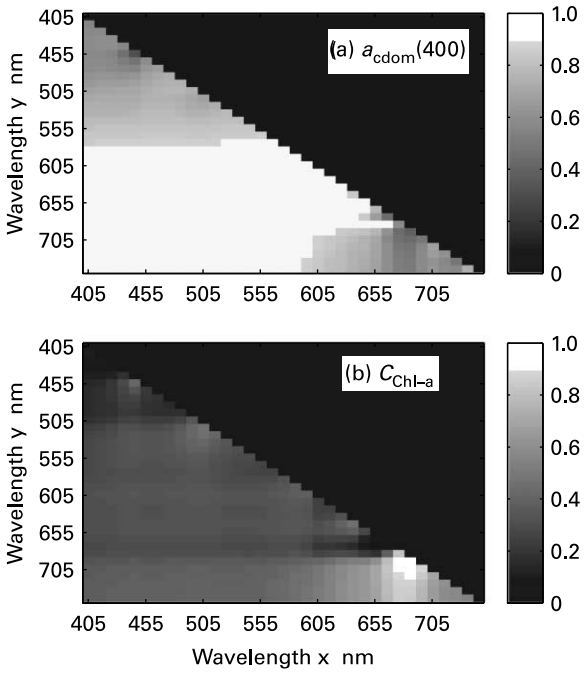


**Figure 9** Surface plot of coefficient of determination ($R^2$) for all possible 10 nm channel ratios of reflectance vs. $a_{cdom}(400)$ (a) and $C_{Chl\text{-}a}$ (b) in the low CDOM sub-group ($N = 797$) of the oligotrophic lakes. $R^2$ is indicated in gray scale and point($x$,$y$) is $R^2$ for the channel ratio $y/x$

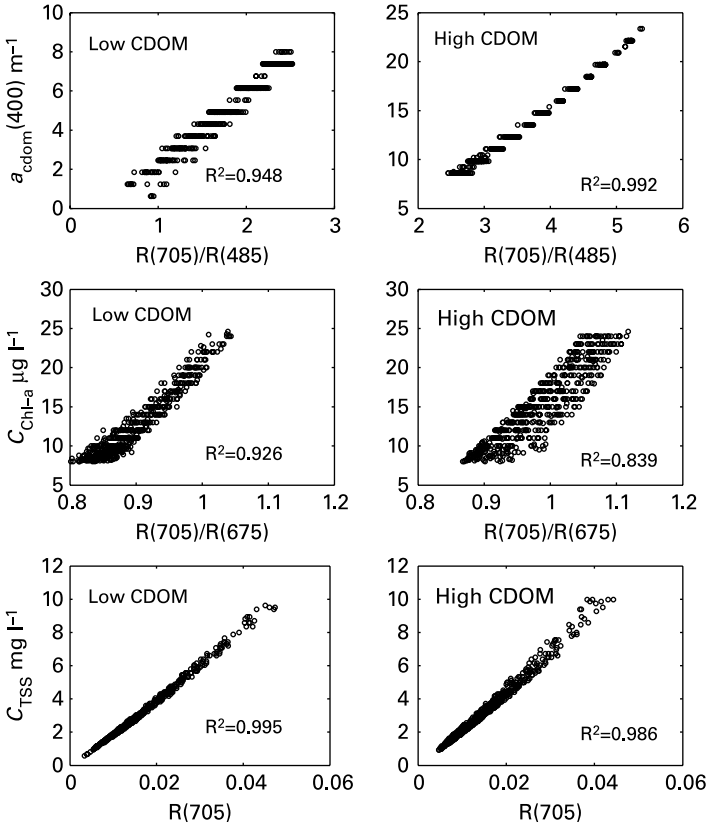


**Figure 10** Correlations between simulated channel ratios and measured OAS in the low (left column, $a_{cdom}(400) < 8.61\ m^{-1}$, $N = 547$) and high (right column, $a_{cdom}(400) > 8.61\ m^{-1}$, $N = 608$) CDOM sub-groups in the mesotrophic lakes. $C_{TSS}$ was estimated from turbidity

The high number of simulated $R(\lambda)$ enables the investigation of the algorithm performance at different trophic and CDOM levels, which is not possible with a small dataset of measured $R(\lambda)$. For example, $R^2$ of the Chl *a* algorithm is lower in the high CDOM than in the low CDOM sub-groups in all trophic classes (Table 6). Although CDOM absorption in the 660–680 nm region is small (Figure 6), it disturbs the $C_{chl\text{-}a}$ algorithm by decreasing $R$ in the 660–680 nm region at high CDOM. This leads to higher NIR/Red ratios and to overestimation of $C_{chl\text{-}a}$ if an algorithm calibrated for low CDOM is applied. The impact of CDOM on the NIR/Red ratio-based Chl *a* algorithm was shown earlier in three Swedish lakes by Pierson and Strömbeck (2000) and Strömbeck and Pierson (2001). However, the disturbing effect of CDOM on the Chl *a* estimation is the weaker the higher the trophic level (Table 6, Figure 10). This is probably due to the fact that CDOM absorption in the 660–680 nm region is low compared with the high phytoplankton absorption.

According to the simulation results, the accuracy of the Chl *a* estimation by remote sensing for a large group of lakes is higher if the CDOM variation is small. When applying the NIR/Red ratio for Chl *a* estimation of lakes with high CDOM variation, the Chl *a* algorithm could be corrected for the impact of CDOM absorption by using the bio-optical reflectance model. The CDOM level of each lake/station required for the correction can be obtained from previous monitoring results or estimated from the remote sensing data. The CDOM level did not influence substantially the $C_{TSS}$ and $a_{cdom}(400)$ estimation accuracy in any trophic class (Table 6, Figure 10).

The estimation accuracies of the empirical water quality algorithms are also influenced by the variation of SIOPs. The SIOPs in the simulations were fixed and their values were based on the measurements at a few lakes. In reality, the SIOPs can vary temporally, from lake to lake and even within the same lake (e.g. Strömbeck and Pierson 2001). For example, the accuracy of the $C_{TSS}$ algorithm based on $R(705)$ depends on the variation of the specific backscattering coefficient of $C_{TSS}$. $C_{Chl\text{-}a}$ estimation is influenced by the variation of $a_{ph}(\lambda)$, backscattering coefficient of phytoplankton and $S_{cdom}$ (Strömbeck and Pierson 2001). However, the optimum channels for the algorithms are likely to be the same when working with measured $R(\lambda)$ (e.g. Kallio *et al.* 2001), but the estimation accuracy is probably lower. This was also shown in $R$ simulations (Pierson and Strömbeck 2001; Strömbeck and Pierson 2001), in which the observed variation of SIOPs was taken into account.

In this study, the influence of $S_{cdom}$ on the OAS algorithms was also investigated. Determination of $S_{cdom}$ is not standardized and the methods applied differ in wavelength range, filter type and pore size used in the filtering of water samples, and in the method of correcting spectrophotometric measurements for residual scattering. The $S_{cdom} = 0.015\,nm^{-1}$ used in the simulations was based on the measured $a_{cdom}(\lambda)$ (SALMON dataset), which were corrected for residual scattering by the subtraction of $a_{cdom}(750)$ from the $a_{cdom}$ at $<750$ nm. Another study consisting of 108 $a_{cdom}(\lambda)$ measurements in Finnish lakes yielded $s_{cdom} = 0.0169$ (Sipelgas *et al.* 2003), when the residual scattering correction was performed according to Bricaud *et al.* (1981). This method assumes that scattering correction increases with decreasing wavelength. Next, the impact of a higher $S_{cdom}$ ($0.017\,nm^{-1}$) on the empirical algorithms was tested. Chl *a* was the most sensitive of the three OAS to the variation in $S_{cdom}$. The increase in $R^2$ was greatest in the high CDOM sub-groups. For example, $R^2$ between $C_{Chl\text{-}a}$ and $R(705)/R(675)$ increased in the high CDOM sub-group of oligotrophic lakes from 0.76 to 0.88. The best $a_{cdom}(400)$ and $C_{TSS}$ algorithms (Table 6) were not sensitive to $S_{cdom}$ as the changes in $R^2$ were negligible.

In the present study, $C_{TSS}$ was estimated from turbidity and $a_{cdom}(400)$ from Pt water colour. The Pt water colour determination is a suitable measure of CDOM, particularly in humic lakes. In eutrophic lakes other OAS (e.g. detritus, inorganic particles, phytoplankton) which affect water colour may disturb the determination. Another problem is that the precision of the method is low in clear water lakes with low water colour ($<15\,mgPt\,l^{-1}$). In these lakes the water is typically green or blue rather than brown/yellow and it is difficult to obtain a Pt colour match (e.g. Davies-Colley *et al.* 2003). Moreover, the Pt water colour values are not continuous due to the use of standard disks (EN ISO 7887:1994). The three lowest values that can be determined by this method in Finnish water laboratories are 2.5, 5 and $10\,mgPt\,l^{-1}$ corresponding to $a_{cdom}(400)$ of 0.31, 0.62 and $1.23\,m^{-1}$, respectively. For example, in the ultra-oligotrophic Lake Vasikkajärvi (Table 1) the simulated $R(400)$ decreased from 0.0094 to 0.0053, when the Pt colour based $a_{cdom}(400)$ estimate ($0.062\,m^{-1}$) is used instead of the measured value ($0.031\,m^{-1}$).

Nephelometric turbidity is a relative measure of light (860 nm) scattered within a 90° angle from a beam directed at the water sample. The ratio between turbidity and $C_{TSS}$ can vary depending on the type of particles and their scattering properties.The comparison of the use of measured $C_{TSS}$ concentrations vs. $C_{TSS}$ calculated from turbidity in the optical models was carried out employing the SALMON dataset, in which the measured $K_d(\lambda)$, $Z_{SD}$ and $R(\lambda)$ were available. The simulations with $C_{TSS}$ calculated from turbidity were performed with the model coefficients described in this paper, and the simulated values were compared with the measured $K_d(\lambda)$, $Z_{SD}$ and $R(\lambda)$. The rmse of $K_d$ simulations ranged between 9.7 and 20.6% (mean 17.6%, $N = 7$), which is close to the rmse of the $C_{TSS}$-based simulations (9.9–21.1%, mean 15.8%). For the $Z_{SD}$ model with $C_{TSS}$ estimated from turbidity $R^2$ was slightly higher (0.988, $N = 14$) than for the $C_{TSS}$-based simulations

($R^2 = 0.965$). The rmse of the turbidity-based $R(\lambda)$ simulations was 41.9% ($N = 12$) and $R^2 = 0.83$. The corresponding values for the $C_{TSS}$-based simulations were 24.8% and 0.92. The greatest discrepancies were in the two most eutrophic stations (Sie-a and Loh1-a, with $C_{Chl\text{-}a} \geq 55\,\mu g\,l^{-1}$ and $C_{TSS} \geq 16\,mg\,l^{-1}$), where the simulated $R(\lambda)$ were higher than those of the $C_{TSS}$-based simulations. The exclusion of these stations resulted in rmse = 34.5% and $R^2 = 0.88$.

This test with limited data suggests that the use of turbidity as a measure of $C_{TSS}$ has little influence on the $K_d$ and $Z_{SD}$ simulations or on $R(\lambda)$ of the oligo-mesotrophic lakes. In the eutrophic lakes of this study the ratio between turbidity and $C_{TSS}$ differs from that in the other lakes, which explains the differences in $R(\lambda)$. The different backscattering properties in the eutrophic lakes as compared to the other SALMON lakes can be due to, for example, high biomass of cyanobacteria, as was earlier discussed by Kallio *et al.* (2005), for example. For the needs of bio-optical modeling, it would be best to determine the concentrations of the main fractions of TSS (inorganic SS, detritus, phytoplankton) and to use their specific spectral scattering and backscattering properties.

The development of optical models would benefit if more optical measurements (e.g. spectral upwelling and downwelling irradiance, $a_{tot}$, $b_{tot}$, $bb_{tot}$, $a_{ph}$, $a_{cdom}$) were included in routine monitoring. This requires suitable optical instruments and time for making the measurements. If this is not possible, the SIOPs should be investigated in representative lakes. Optical and remote sensing applications require correct laboratory determinations of OAS concentrations for algorithm calibration and validation. In Finland, determinations of $a_{cdom}(400)$, TSS and inorganic SS have been included in the national monitoring of lakes and coastal regions since 2000. National monitoring covers all the large lakes in Finland and involves 71 stations, of which 15 have intensive sampling.

## Conclusions

Optical models calibrated using optical measurements of 10 lakes were combined with nationwide monitoring results from 1670 stations, for which OAS concentrations were available. This enabled the calculation of $K_d(\lambda)$ and $R(\lambda)$ for the whole of Finland. These optical properties are laborious to measure in the field. In practice, the approach applied here is the only way to estimate $K_d(\lambda)$ and $R(\lambda)$ in lake-rich countries such as Finland. The approaches presented can be used for any region for which OAS concentrations, SIOPs and calibrated optical models are available. The $Z_{SD}$, $K_d(\lambda)$ and $R$ models can be used in lake management, in hydrodynamic ecosystem models, in estimating light available for photosynthesis and in various remote sensing applications.

The simulation of $R$ using typical variations of OAS is a valuable tool in the preliminary development and evaluation of remote sensing algorithms. Finnish lakes are characterized by high $a_{cdom}(400)$. According to the simulation results high $a_{cdom}(400)$ decrease the estimation accuracy of $C_{Chl\text{-}a}$ by the NIR/Red ratio, particularly in oligothrophic lakes, whereas the accuracy of the $a_{cdom}(400)$ and $C_{TSS}$ algorithms did not depend on the $a_{cdom}(400)$ level. The estimation of $C_{Chl\text{-}a}$ can also be sensitive to the variation of $S_{cdom}$. Methods that take into account the disturbing effect of $a_{cdom}(400)$ levels and $S_{cdom}$ variation on the $C_{Chl\text{-}a}$ estimation should be developed further. Spectral attenuation depths combined with bathymetric maps can be used to identify locations where reflection from the bottom disturbs the estimation of water quality, which is an important consideration for developing reliable remote sensing products.

Obviously the model coefficients in a particular lake may be different from those assumed here. The estimation accuracy of $K_d(\lambda)$, $Z_{att}(\lambda)$ and $R(\lambda)$ could be improved if more measurements of the optical properties were available for model calibration and validation. Therefore, the SIOPs and other model coefficients should be further surveyed to determine their regional and seasonal variation.

## Acknowledgements

The optical measurements were part of the Satellite Remote Sensing for Lake Monitoring (SALMON) project funded by the European Union (ENV4-CT96-0311). The Academy of Finland is acknowledged for their financial support (Development of Methods to Apply Earth Observation Data in the Monitoring of Water Quality in the Baltic Sea and Lakes-project, SA104901).



## References

Bricaud, A., Morel, A. and Prieur, L. (1981). Absorption by dissolved organic matter of the sea (yellow subtance) in the UV and visible domains. *Limnol. Oceanogr.*, **26**, 43–53.

Buiteveld, H., Hakvoort, J.H.M. and Donze, M. (1994). The optical properties of pure water. *Proceedings of the Ocean Optics XII Conference, SPIE*, **2258**, 174–183.

Bukata, R.P., Jerome, J.H. and Bruton, J.E. (1988). Relationships among Secchi disc depth, beam attenuation coefficient for Great Lakes waters. *J. Great Lakes Res.*, **14**, 347–355.

Bukata, R.P., Jerome, J.H., Bruton, J.E. and Jain, S.C. (1979). Determination of inherent optical properties of Lake Ontario coastal waters. *Appl. Opt.*, **18**, 3926–3932.

Davies-Colley, R.J. (1988). Measuring water clarity with a black disk. *Limnol. Oceanogr.*, **33**, 616–623.

Davies-Colley, R.J., Vant, W.N. and Smith, D.G. (2003). *Colour and Clarity of Natural Waters. Science and Management of Optical Water Quality*, The Blackburn Press, Caldwell, NJ.

Dekker, A.G. (1993). *Detection of optical water quality parameters for eutrophic waters by high resolution remote sensing*. PhD Thesis, Vrije Universiteit, Amsterdam, The Netherlands.

Doerffer, R. and Fischer, J. (1993). Concentrations of chlorophyll, suspended matter and gelbstoff in case II waters derived from satellite Coastal Zone Scanner data with inverse modeling. *J. Geophys. Res.*, **99**, 7457–7466.

Effler, S.W., Gelda, R.K., Bloomfield, J.A., Quinn, S. and Johnson, D.L. (2001). Modeling the effects of tripton on water clarity: Lake Champlain. *J. Wat. Res. Plann. Mngmnt.*, **127**, 224–234.

Effler, S.W. and Perkins, M.G. (1996). An optics model for Onondaga Lake. *Lake Reservoir Mngmnt.*, **12**(1), 115–125.

Effler, S.W., Perkins, M.G., Ohrazha, N., Matthews, D.A., Gelda, R., Peng, F., Johnson, D.L. and Stephckuz, C.L. (2002). Tripton, transparency and light penetration in seven New York reservoirs. *Hydrobiologia*, **468**, 213–232.

EN 872 (1996). *Water Analysis – Determination of Suspended Solids*. European Committee for Standardization, Strasbourg.

EN 27027 (1994). *Water Quality - Determination of Turbidity*. European Committee for Standardization, Strasbourg.

EN ISO 7887 (1994). *Water Quality. Examination and Determination of Colour*. International Standards Organization, Geneva.

EN ISO/IEC 17025 (1999). *General Requirements for the Competence of Testing and Calibration Laboratories*. International Standards Organization. Geneva.

Gitelson, A., Garbuzov, G., Szilagyi, F., Mittenzwey, K.-H., Karnieli, K. and Kaiser, A. (1993). Quantitative remote sensing methods for real-time monitoring of inland waters quality. *International Journal of Remote Sensing*, **14**, 1269–1295.

Gordon, H.R., Brown, O.B. and Jacobs, M.M. (1975). Computed relationships between the inherent and apparent optical properties of a flat, homogenous ocean. *Appl. Opt.*, **14**, 417–427.

Härmä, P., Vepsäläinen, J., Hannonen, T., Pyhälahti, T., Kämäri, J., Kallio, K., Eloheimo, K. and Koponen, S. (2001). Detection of water quality using simulated satellite data and semi-empirical algorithms in Finland. *Sci. Total Environ.*, **268**, 107–121.

Herlevi, H. (2002). Inherent and apparent optical properties in relation to water quality in Nordic waters. PhD Thesis, University of Helsinki, Report Series in Geophysics, 45.

Holmes, R.W. (1970). The Secchi disk in turbid coastal waters. *Limnol. Oceanogr.*, **15**, 688–694.

Hoogenboom, H.J., Dekker, A.G. and De Haan, J.F. (1998). Retrieval of chlorophyll a and suspended matter in inland waters from CASI data by matrix inversion. *Can. J. Remote Sensing*, **24**, 144–152.

Huttula, T., Peltonen, A., Bilaletin, A. and Saura, M. (1992). The effects of climatic change on lake ice and water temperature. *Aqua Fennica*, **22**, 129–142.

ISO 10260 (1992). *Water Quality – Measurement of Biochemical Parameters – Spectrometric Determination of the Chlorophyll a Concentration*. International Organization for Standardization, Geneva.

Jasby, A.D., Goldman, C.R., Reuter, J.E. and Richards, R.C. (1999). Origins and scale dependence of temporal variability in the transparency of Lake Tahoe, California – Nevada. *Limnol. Oceanogr.*, **44**, 282–294.

Jerlov, N.G. (1976). *Marine Optics*. Elsevier, Amsterdam.

Kallio, K., Koponen, S. and Pulliainen, J. (2003). Feasibility of airborne imaging spectrometry for lake monitoring - a case study of spatial chlorophyll a distribution in two meso-eutrophic lakes. *Int. J. Remote Sensing*, **24**, 3771–3790.

Kallio, K., Kutser, T., Hannonen, T., Kutser, T., Koponen, S., Pulliainen, J., Vepsäläinen, J. and Pyhälahti, T. (2001). Retrieval of water quality variables from airborne spectrometry of various lake types in different seasons. *Sci. Total Environ.*, **268**, 59–77.

Kallio, K., Pulliainen, J. and Ylöstalo, P. (2005). MERIS, MODIS and ETM channel configurations in the estimation of lake water quality from subsurface reflectance with semi-analytical and empirical algorithms. *Geophysica*, **41**, 31–55.

Kirk, J. (1984a). Dependence of relationship between inherent and apparent optical properties of water on solar altitude. *Limnol. Oceanogr.*, **29**, 350–356.

Kirk, J. (1984b). Attenuation of solar radiance in scattering-absorbing water, a simplified procedure for its calculation. *Appl. Optics*, **23**, 3737–3739.

Kirk, J. (1994). *Light and photosynthesis in aquatic ecosystems*, Cambridge University Press.

Koponen, S., Pulliainen, J., Servomaa, H., Zhang, Y., Hallikainen, M., Kallio, K., Vepsäläinen, J., Pyhälahti, T. and Hannonen, T. (2001). Analysis on the feasibility of multi-source remote sensing observations for chl-a monitoring in Finnish lakes. *Sci. Total Environ.*, **268**, 95–106.

Kutser, T., Pierson, D.C., Tranvik, L.J., Reinart, A., Sobek, S. and Kallio, K. (2005). Estimating the colored dissolved organic matter absorption coefficient in lakes using satellite remote sensing. *Ecosystems*, **8**, 709–720.

Maffione, R.A. and Dana, D.R. (1996). Recent measurements of the spectral backward-scattering coefficient in coastal waters. *Proceedings of the Ocean Optics XIII, SPIE*, **2963**, 154–159.

Maffione, R.A. and Jaffe, J.S. (1995). The average cosine due to an isotropic light source in the ocean. *J. Geophys. Res.*, **100**, 13179–13192.

Millie, D.F., Baker, M.C., Tucker, C.S., Vinyard, B.T. and Dionogi, C.P. (1992). High-resolution airborne remote sensing of bloom-forming phytoplankton. *Journal of Phycology*, **28**, 281–290.

Morel, A. (1988). Optical modeling of the upper ocean in relation to its biogenous matter content (case I waters). *J. Geophys. Res.*, **93**, 10749–10768.

OECD (1982). *Eutrophication of Water. Monitoring, Assessment and Control*. OECD, Paris.

Pierson, D.C. and Strömbeck, N. (2000). A modelling approach to evaluate preliminary remote sensing algorithms: Use of water quality data from Swedish Great Lakes. *Geophysica*, **36**, 177–202.

Pierson, D. and Strömbeck, N. (2001). Estimation of radiance reflectance and the concentrations of optically active substances in Lake Mälaren, Sweden, based on direct and inverse solutions of a simple model. *Sci. Total Environ.*, **268**, 171–188.

Pozdnyakov, D.V., Kondratyev, K.Ya, Bukata, R.P. and Jerome, J.H. (1998). Numerical modeling of natural colour: implications for remote sensing and limnological studies. *Int. J. Remote Sensing*, **19**, 913–932.

Preisendorfer, R.W. (1986). Secchi disk science; visual optics of natural waters. *Limnol. Oceanogr.*, **31**, 906–926.

Pulliainen, J., Kallio, K., Eloheimo, K., Koponen, S., Servomaa, H., Hannonen, T., Tauriainen, S. and Hallikainen, M. (2001). A semi-operative approach to water quality retrieval from remote sensing data. *Sci. Total Environ.*, **268**, 79–93.

Raatikainen, M. and Kuusisto, E. (1990). The number and surface area of lakes in Finland (in Finnish with English abstract). *Terra*, **102**(2), 97–110.

Reinart, A., Arst, H., Erm, A., Trei, T. and Hussainov, M. (2001). Optical and biological properties of Lake Ülemiste, a water reservoir of the city of Tallinn II: Light climate in Lake Ülemiste. *Lakes Reservoirs Res. Mngmnt.*, **6**, 75–84.

Rijkeboer, M., Dekker, A.G. and Gons, H.J. (1998). Subsurface irradiance reflectance spectra of inland waters differing in morphometry and hydrology. *Aquat. Ecol.*, **31**, 313–323.

Roesler, C.S., Perry, M.J. and Carder, K.L. (1989). Modeling in situ phytoplankton absorption from total absorption spectra. *Limnology and Oceanography*, **34**, 1512–1525.

Sathyendranath, S., Prieur, L. and Morel, A. (1989). A three component model of ocean colour and its application to remote sensing of phytoplankton pigments in coastal waters. *International Journal of Remote Sensing*, **10**, 1373–1394.

Schalles, J.F., Gitelson, A.A., Yacobi, Y.Z. and Kroenke, A.E. (1998). Estimation of chlorophyll *a* from time series measurements of high spectral resolution reflectance in a eutrophic lake. *Journal of Phycology*, **34**, 383–390.

Sipelgas, L., Arst, H., Kallio, K., Erm, A., Oja, P. and Soomere, T. (2003). Optical properties of dissolved organic matter in Finnish and Estonian lakes. *Nordic Hydrol.*, **34**, 361–386.

Strömbeck, N. and Pierson, D. (2001). The effects of variability in the inherent and optical properties on estimations of chlorophyll a by remote sensing in Swedish freshwaters. *Sci. Total Environ.*, **268**, 123–137.

Tyler, J.E. (1968). The Secchi disk. *Limnol. Oceanogr.*, **13**, 1–6.

Umgiesser, G., Luyten, P.J. and Carniel, S. (2002). Exploring the thermal cycle of the Northern North Sea area using a 3-D circulation model: the example of PROVESS NNS station. *J. Sea Res.*, **48**, 271–286.

Van Duin, E.H.S., Blom, G., Los, F.J., Maffione, R., Zimmerman, R., Cerco, C.F., Dortch, M. and Best, E.P.H. (2001). Modeling underwater light climate in relation to sedimentation, resuspension, water quality and autotrophic growth. *Hydrobiologia*, **444**, 25–42.

Vant, W.N. and Davies-Colley, R.J. (1984). Factors affecting clarity of New Zealand lakes. *New Zealand J. Marine Freshwater Res.*, **18**, 367–377.

Ylöstalo, P., Kallio, K. and Seppälä, J. (2005). Absorption properties of particles and CDOM in lake waters, (in preparation).